Journal of Alloys and Compounds 1039 (2025) 182861

Contents lists available at ScienceDirect

Journal of Alloys and Compounds

journal homepage: www.elsevier.com/locate/jalcom

Local strain field evolution at shot-peened 7075 Al-base notches upon tensile loading using in-situ synchrotron X-ray μ-diffraction

Aitor Madariaga [a,b,*], Eduardo Vazquez [c], Daniel Foster [a,d], Enrique Jimenez-Melero [e,**]

[a] Department of Materials, University of Manchester, Oxford Road, Manchester M13 9PL, UK
[b] Mondragon Unibertsitatea, Engineering Faculty, Loramendi 4, Arrasate-Mondragon 20500, Spain
[c] Ipar-Blast SL, Parque industrial Itziar-Deba, Parcela 4, pabellón F2-5, Itziar, Gipuzkoa 20829, Spain
[d] NanoTerasu Promotion Division, Japan Synchrotron Radiation Research Institute (JASRI), 468-1, Aramaki Aza Aoba, Sendai, Miyagi 980-8572, Japan
[e] School of Metallurgy and Materials, University of Birmingham, Edgbaston, Birmingham B15 2TT, UK

ARTICLE INFO

Keywords:
Aluminium alloys
Shot peening
Synchrotron X-ray diffraction
Finite element modelling
Micromechanics
Aerospace

ABSTRACT

Shot peening (SP) is commonly applied to Al-base alloys during manufacture to enhance their fatigue tolerance and notch sensitivity in aerospace engineering components with geometrical discontinuities. We have mapped with high spatial resolution the local strain field induced by surface shot peening around notches in aerospace 7050-T7451 alloy, and determined the local mechanical behaviour of the surface affected layer during room-temperature tensile testing. For this purpose, we have performed in-situ synchrotron X-ray μ-diffraction during tensile loading of notched specimens in the as-machined condition, and also for two different shot peening intensities. The behaviour of the notched specimen not affected by machining and SP was also simulated by finite element modelling to decouple the local surface mechanical response from the bulk material behaviour. The results confirmed that shot peening induces compressive residual stresses close to the notch tip, and also changes in notch geometry and surface topography. Shot-peened surfaces experience accommodation of plastic effects at the early stages of the tensile test, and they yielded at ~70–80 % higher applied nominal tensile stresses than the as-machined material. When increasing the applied stress, the maximum longitudinal elastic strain shifts beneath the surface, and the magnitude of the peak strain and its position converge to the same value for the as-machined and shot-peened specimens. Beyond yielding, there is an exponential increase in plastic strain close to the notch tip, irrespective of the initial surface condition. The overall elasto-plastic response of the material is not affected by shot peening, but compressive residual strains significantly retard yielding close to the notch tip under loading.

1. Introduction

Aluminium base alloys are likely the most used materials for vehicle weight reductions, due to their light weight, good formability, static strength, and corrosion resistance [1]. However, Al-base alloys possess low elasticity and fatigue strength, those being critical when manufacturing structural components with geometrical discontinuities that must withstand cyclic loads in-service, such as aircraft frames. For instance, the high-cycle fatigue endurance of the alloy is ~25 % lower than the tensile strength [2]. Conventional Al-base alloys also show high notch fatigue sensitivity, and their fatigue strength reduces even more when increasing the stress concentration of the notch [3]. To overcome those limitations, surface mechanical treatments, e.g. Shot Peening (SP), are applied in the last stage of the manufacturing chain of Al-based aerospace components. SP consists of projecting hard spheres or shots of small diameter at high speed onto a ductile material's surface [4,5]. The efficiency of peening processes depends on the mechanical energy transferred to the material through the impacts of the shots [6], and the final properties of the SP-affected layer can be controlled by the SP intensity, the peening coverage and shot characteristics [7].

Compressive residual stresses induced by SP reduce the short crack growth rate of notched Al-base alloy, and therefore extends the fatigue life, as compared to the non-peened condition [8,9]. Although the crack initiation can be shorter in shot-peened surfaces [8], this only takes a small percentage of the whole fatigue life [9]. Furthermore, the SP effectiveness in improving the fatigue strength of components with

* Corresponding author at: Department of Materials, University of Manchester, Oxford Road, Manchester M13 9PL, UK.
** Corresponding author.
E-mail addresses: aitor.madariaga@manchester.ac.uk (A. Madariaga), e.jimenez-melero@bham.ac.uk (E. Jimenez-Melero).

https://doi.org/10.1016/j.jallcom.2025.182861
Received 13 June 2025; Received in revised form 31 July 2025; Accepted 6 August 2025
Available online 7 August 2025

geometrical discontinuities is higher than in smooth components [10,11]. For instance, Benedetti et al. [11] demonstrated in 7075-T651 alloy that the effectiveness of SP is higher in sharp notches (stress concentration, $k_t = 2.33$) than in blunt notches ($k_t = 1.53$). Later, they performed pulsating bending fatigue tests ($R = 0.05$) of shot-peened smooth and notched samples ($k_t = 1.5$, 2.3 and 3.7) of 7075-T651 alloy to assess how residual stresses affect the very high cycle regime (10^5-10^8 cycles) [12,13]. Sharp notches showed higher concentration of residual stresses at the notch tip and led to a remarkable improvement of the fatigue strength, whereas the beneficial effect of blunt notches diminished with increasing fatigue cycles. Recently, Jambor et al. [14] analysed the effect of severe SP on the very high cycle fatigue ($R = -1$) of notched ($k_t = 2.45$) AW 7075 alloy. They found that severe SP improved by 15 % the fatigue strength of non-peened samples in the range of 10^7-10^9 loading cycles. However, severe SP decreased the fatigue life when higher mechanical stresses were applied, due to the relaxation of compressive residual stresses and the impact of surface roughness on crack initiation. Relaxation of compressive residual stresses during fatigue loading of notched specimens was also reported by Benedetti et al. [12], highlighting the necessity to monitor the stability of residual stresses.

The development of reliable fatigue models can alternatively minimise the need for experimental data over a wide range of notch geometries, SP conditions and loading parameters. In this respect, Mutoh et al. [8] predicted the fatigue crack growth of notched Al-base specimens, including experimental data of the residual stress distribution and data for crack growth rate of a non-peened specimen. Benedetti et al. [5] proposed instead a simplified fatigue life prediction model of notched 7075-T651 specimens, applying a multiaxial criterion and the Theory of Critical Distance (TCD) that considers the stabilised residual stress field. Later, they also applied the Crossland criteria and TCD, including the SP-induced residual stresses, to estimate the fatigue life of notched specimens subjected to pulsating loads in the very high cycle regime [13]. Recently, Bagherifard et al. [10,15], compared different fatigue prediction models for shot-peened notched specimens, and they also concluded that TCD provides accurate results, since it also considers the alterations of SP condition and the potential relaxation of residual stresses during the load cycles.

Despite this body of work, for a robust notch fatigue assessment of shot-peened Al-base components, it is mandatory to consider the initial residual stress field around the notch and its stability [16]. Unfortunately, the measurement of SP-induced residual stress fields around sharp notches remains experimentally challenging. Some authors have derived in-depth residual stresses at the notch tip using laboratory X-ray diffraction combined with electropolishing steps to remove layers [8,9,14]. However, standard X-ray diffractometers use beam sizes > 0.5 mm^2, which cannot help to resolve high residual stress gradients around sharp notches, and electropolishing in those constraint geometries can alter the SP-induced residual stress distribution. Interestingly, Winiarski et al. [17] used μ-XRD and FIB-SEM DIC micro-slot cutting and micro-hole drilling to measure residual stresses with a spatial resolution of ~50 μm, but only along the bisector of the notch. Later, Benedetti et al. [18] combined those measurements and Finite Element Modelling (FEM) to reconstruct the residual stress field around sharp and blunt notches. Moreover, sub-surface stresses could be determined with higher accuracy by neutron and/or synchrotron X-rays diffraction [9,19]. The mechanical response of the SP-affected surface layer can be best monitored in situ by X-ray diffraction under mechanical loading [20–23], with synchrotron X-rays opening the door to measuring the local response around notches and cracks with adequate spatial resolution [24–26]. To the best of our knowledge, there are no reports in the literature that have used this approach to determine the changes in local mechanical response within shot-peened notched surfaces in Al-base alloys.

The aim of this work is therefore to map, with high spatial resolution using synchrotron X-rays, the SP-induced residual strain field around notches in 7050-T7451 alloy, and thereupon assess the impact on the local mechanical behaviour of the SP-affected thin layer upon tensile loading. This is a necessary stepping stone in assisting the development and validation of reliable fatigue models in SP-affected Al-base alloys with geometrical discontinuities. Complementarily to the in-situ synchrotron X-ray diffraction experiment under loading, finite element simulations of the bulk material under test were carried out to predict the behaviour of a notch not affected by finishing operations such as shot peening or machining. This allowed us to decouple the local response of the SP-affected layers from the non-peened, bulk material behaviour. This procedure has not yet been explored to map the local variation in mechanical response of notches treated by shot peening.

2. Experimental

2.1. Materials

Table 1 shows the chemical composition of the as-received 7050-T7451 rolled plate, determined by Inductively Coupled Plasma spectroscopy. This alloy is widely used in the production of thin-walled structural components of aircrafts. Rectangular flat specimens ($38 \times 16 \times 1.5$ mm^3) with the geometry shown in Fig. 1a were designed following the good practices for miniaturised tensile tests [27] to ensure that they represent the bulk behaviour of the polycrystal up to the rupture stress: i) thickness (t) to grain size (d) ratio $t/d = 13.6 > 10$ and ii) width (w) to thickness ratio $w/t = 1.7 < 5$. The specimens were initially extracted from the as-received plate using a high precision saw. The longest specimen dimension was aligned with the rolling direction of the plate. Afterwards, the contour of the tensile specimens was milled to obtain the final geometry of the notched specimen shown in Fig. 1a. Smooth conditions were used to avoid inducing high surface residual stresses and deforming the microstructure near the surface. The specimens' cross section was verified during the manufacturing process using a calliper, and the diameter of the notches using an optical microscope to ensure that dimensional tolerance was below 0.05 mm. Test specimens cross section showed a deviation < 6 % between different specimens.

Shot peening was finally applied to the notched side of the specimens, see Fig. 1a, using a NORBLAST S8014SHOT pneumatic shot peening machine. S110 steel shots of 300 μm diameter were used to impact the material's surface with a coverage > 125 %. The diameter of the shots was 4 times higher than the diameter of the notch, and 5 times than of the thickness. In practice, it rapidly reaches a coverage > 125 % when treating a 1.2 mm diameter notch. We used a magnifying glass to inspect the shot-peened surfaces and coverage was calculated following the SAE J2277 standard [28], exposing the specimens to shots > 1.25 times the exposure time necessary to achieve 98 % coverage. Equivalent specimens were treated using two different SP intensities, as summarised in Table 2. Low intensity Shot Peening (LSP) conditions employed a flow of 9.93 kg/min, pressure of 1.5 bar and Almen intensity of 3.4 A. The pressure and intensity were raised to 4 bar and 10.9 A to manufacture High intensity Shot Peening specimens (HSP). Almen intensity specification and test specimen thickness are not directly related. In this case, 3.4 A (0.085 mm) and 10.9 A (0.27 mm) intensities are correctly measured with A type Almen strips, as A type is recommended for intensities below 20.4 (0.51 mm arc height). The test specimen thickness was 1.5 mm; enough to be treated with the mentioned intensities. These conditions were satisfactorily used in [29].

The characterisation of the as-received and shot-peened microstructure was reported in [29]. The bulk microstructure contained a combination of fine grains (average size of 6 μm) and coarser grains (average size of 110 μm). There is ~ 1 vol% of secondary phases (mainly Al_7Cu_2Fe and Mg_2Si) with a grain size varying from 1–2 to 30 μm, located predominantly within the coarse-grained areas of the matrix. The microstructure and surface topography of the as-machined (AM) and shot-peened surfaces were characterised to ensure that different surface conditions were induced in the notched specimens. Small coupons were extracted out from areas in the microstructure close to the

Table 1
Chemical composition (in wt%) of the as-received 7050-T7451 rolled plate.

V	Si	Fe	Cu	Mn	Mg	Cr	Zn	Ti	Zr	Other	Al
0.01	0.02	0.06	1.87	0.01	2.00	0.01	6.22	0.02	0.11	< 0.01	Bal.

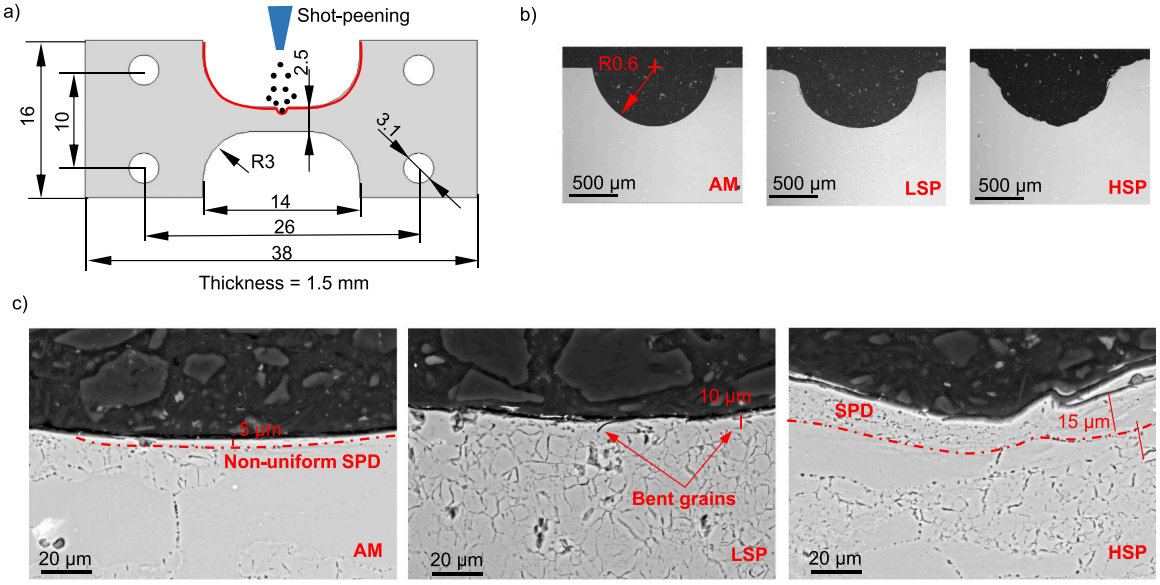

Fig. 1. (a) Geometry of the notched tensile specimen and schematic of the shot peening process of the notched side; (b) low magnification images of the notch cross section in the As-Machined (AM), Low (LSP) and High intensity Shot Peening (HSP) conditions. Shot peening intensity defined by Almen intensity in brackets. (c) backscattered electron images of the notch tip showing the surface topography and the local microstructure. The dashed red line contours the Severe Plastic Deformation (SPD) layer at the specimen surface.

Table 2
Parameters used for the surface treatment of the notch specimens, where LSP stands for Low intensity and HSP for High intensity Shot Peening. The impact energy is quantified by Almen intensity.

Parameter	LSP	HSP
Balls/Shots	S110 (58–60 HRC)	S110 (58–60 HRC)
Flow (kg/min)	9.93	6.97
Pressure (bar)	1.5	4
Almen Intensity (A)	3.4	10.9
Coverage (%)	> 125	> 125

notched region of the three types of specimens (AM, LSP and HSP), mechanically ground and polished, and chemically etched using a Keller's reagent. A FEI Quanta 250 FEG-SEM scanning electron microscope with a 2 kV accelerating voltage was used for microstructural characterisation.

2.2. *In-situ synchrotron X-ray μ-diffraction upon loading*

Interrupted stepwise tensile tests to fracture of the notched specimens in the AM, LSP and HSP conditions were sequentially carried out at room temperature, using a 2 kN micro-tensile rig placed at the high-energy I12 beamline of the UK Diamond Light Source. Specimens were tested at 0.05 mm/min elongation speed under displacement control mode. During the beginning of the elastic loading, loading steps of 0.1 mm were applied, and this was reduced to 0.01–0.02 mm near yielding, while step size was incremented to 0.5 mm for the plastic region. A schematic of the in-situ Synchrotron X-ray Diffraction (SXRD) set-up in transmission geometry can be seen in Fig. 2a. The SXRD geometry was calibrated with a CeO_2 standard [30]. A monochromatic 80 keV ($\lambda = 0.1550$ Å) X-ray beam with a size of 100 × 100 μm^2 illuminated the specimen. The minimum possible beam size (100 × 100 μm^2) was set-up as a compromise between measurement accuracy and spatial resolution. This beam size is suitable for studying the elastic and plastic deformation fields generated by shot peening, since these effects extend to depths up to 500 µm in this study. After each displacement step of ~50 µm in the rig, the specimen was kept at constant displacement and a total Region of Interest (ROI) of 2.0 × 2.5 mm^2 was scanned in steps of 100 µm, see schematic diagram in Fig. 2b. A data acquisition time of 1 Hz was used to collect the 2-D diffraction pattern at each loading step and specimen location in the ROI, using a Thales Pixium RF4343 detector located at a distance of ~630 mm behind the specimen. After the tests, the fracture surface was characterised using a FEI Quanta 250 FEG-SEM microscope.

The lattice strains were analysed in the longitudinal direction ($\varepsilon_{hkl,x}$), since Bagherifard et al. [10] demonstrated that they better represent the fatigue performance of notched specimens treated by SP. It should be clarified that, determined strains for each increment were the average strains through thickness since SXRD experiment was conducted in transmission mode. For this analysis, the recorded 2-D dataset was integrated using the DAWN software package [31] at ± 7.5° azimuthal angle with respect to the loading direction, see Fig. 2a. The resultant 1-D patterns of intensity as a function of scattering angle were analysed using the FullProf Suite software package [32]. Single-peak fitting to a pseudo-Voigt profile function was performed on selected *hkl* reflections, namely 220, 311, 331 and 420, to obtain the position and Full-Width-at-Half-Maximum (FWHM) for each reflection, loading step and position in the ROI. The strains ε_{hkl} for reflection hkl were then determined according to:

$$\varepsilon_{hkl} = \frac{d_{hkl} - d^0_{hkl}}{d^0_{hkl}} \quad (1)$$

where d_{hkl} is the lattice plane spacing at a given loading increment, and d^0_{hkl} at stress free condition. The specimens were scanned before the first

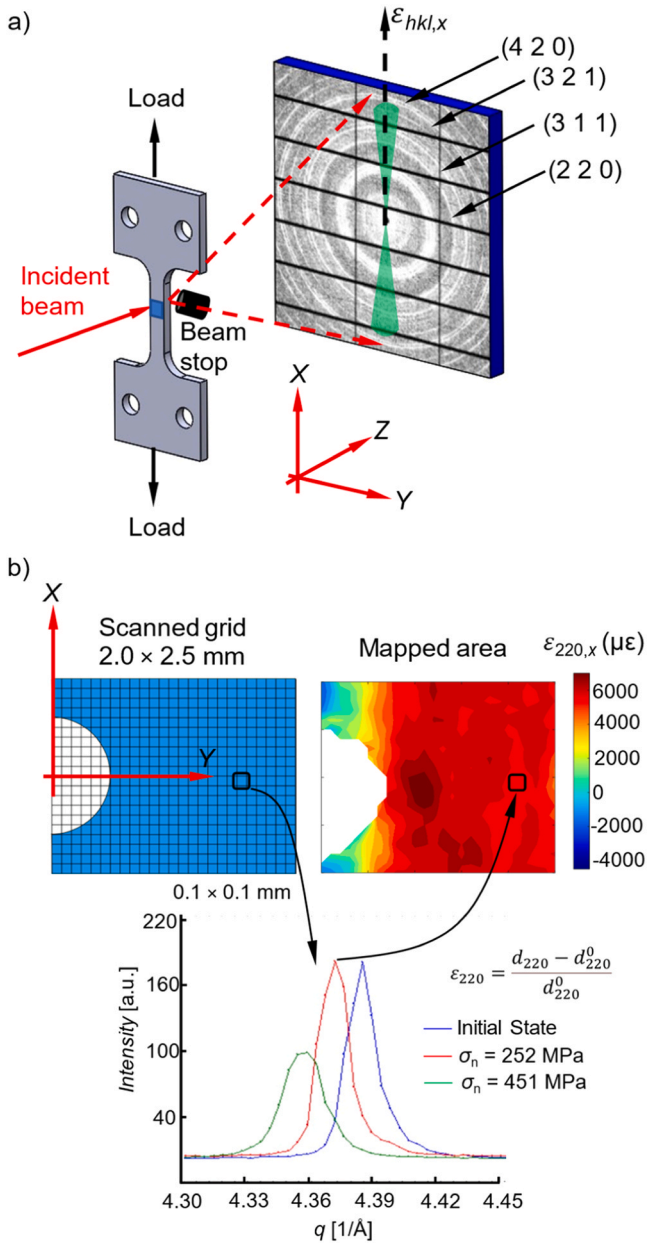

Fig. 2. Schematic of the (a) in-situ synchrotron X-ray diffraction experiment under tensile loading, and (b) scanned grid in the vicinity of the notch, together with an illustrative example of changes in 220 peak position and width upon specimen straining, together with the mapping of longitudinal lattice strains in the as-machined notched specimen at a nominal stress $\sigma_n = 451$ MPa. The region of the 2-D detector where diffracted intensity was used to determine the longitudinal elastic strains is highlighted in green in (a).

load increment, and the lattice plane spacing measured at positions from 1.5 to 2 mm from the notch surface were averaged to determine d^0_{hkl}. Machining and SP did not induce residual stresses at depths greater than 0.5 mm from the surface of the notch. Following this procedure, it was possible to map the distribution of longitudinal elastic strains $\varepsilon_{hkl,x}$ around the notch of the specimens for different applied nominal stresses σ_n, see example in Fig. 2b. The in-depth analysis and discussion hereafter are based on the 220 reflection. However, similar results were obtained for the other reflections under study, see Fig. S.1–3 in supplementary material.

3. Finite element modelling

A simulation of the tensile test of the notched specimen in the absence of initial residual stresses and plastic deformation was done to compare with experimental results in the AM condition, since this condition induced negligible elastic strains near the surface and therefore similar mechanical properties of the bulk material. A 3-D model of the specimen geometry was implemented in the commercial Abaqus Standard finite element software. Fig. 3 shows a 2-D view of this model, together with stress-strain curve of the material which was characterised by tensile tests of unnotched specimens. The material has a Young's modulus $E = 71.4$ GPa, Poisson coefficient $\nu = 0.33$, yield stress $\sigma_y = 436$ MPa and rupture stress $\sigma_u = 500$ MPa. C3D8R-type elements with a general mesh size of 200 μm were implemented in the model, but the mesh size was decreased to 50 μm close to the notch (i.e. half of the step size used to scan the ROI in the SXRD experiment). To reproduce the experiments, the displacement of the specimen holes was restricted in one side of the specimen ($u_x = u_y = 0$), and a displacement $u_{x,\text{applied}} = \Delta$ was applied to the holes along the loading direction. The displacement was incremented stepwise in the simulations, and reaction forces and strains were extracted from the model to compare with the experimental results.

4. Results

4.1. Shot-peened specimens

The low magnification images in Fig. 1b demonstrate that both peening conditions affected the notch geometry. After SP, the notch did not keep after its initial circular shape, and this alteration in notch geometry was more evident when increasing the SP intensity. The transition edge between the radius and the flat region was rounded by the effect of SP. Additionally, the HSP notch showed a rougher surface than the LSP and AM notches, in line with previous observations for unnotched specimens treated under the same SP conditions [29].

Machining processes induce high strains at high strain in the tool-workpiece contact, which can lead to microstructural alterations in aluminium alloys depending on the selected conditions [33]. In this work, smooth conditions were used, and the initial machining of the specimens generated a non-uniform thin layer (<5 μm) with Severe Plastic Deformation (SPD) near one side of the notch tip, see Fig. 1c. The

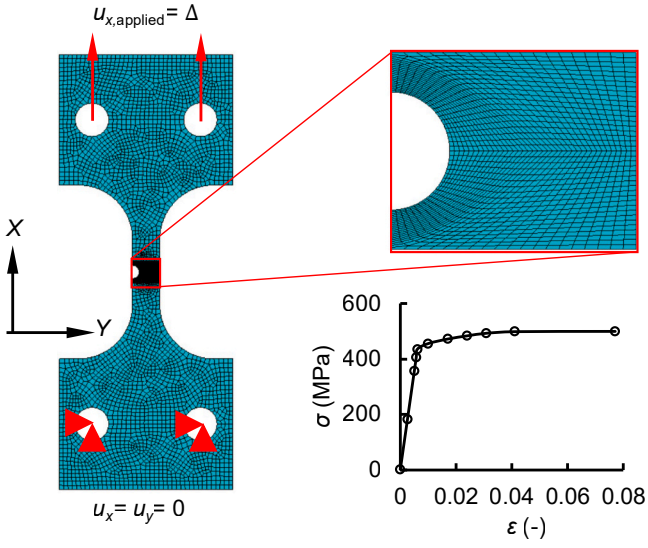

Fig. 3. Geometry of the notched tensile specimen with boundary conditions, details of the mesh in the vicinity of the notch and stress-strain curve used in the finite element simulations.

microstructure near the notch treated by LSP did not evidence significant changes, although some grains near the surface were slightly bent. It is very likely that the SPD produced by machining was a localised effect and not present in all specimens prior to applying shot peening. This could be the main reason to explain the absence of a SPD layer in the LSP sample. However, there is a ~15 μm thick SPD layer as consequence of the increased intensity in the HSP surface, where the fine grain boundaries in the local microstructure appear diffuse. The defects produced by LSP and HSP are consistent with the defects found in [29] under identical conditions. It should be clarified that the thickness of the SPD was < 5 μm in the AM specimen and ~15 μm in the HSP specimen, which is negligible compared to the beam size 100 × 100 μm^2 used in the SXRD experiments. This microstructure modification has also been observed when applying severe SP in aluminium AW 7075 notched specimens [14]. Those near-surface microstructural changes, even causing grain refinement, are more evident when using ultra-fine shots, or significantly increasing coverage above 100 %, as observed by Benedetti et al. [34] in aluminium 7075-T6 specimens.

4.2. Macroscopic behaviour

Fig. 4a shows the nominal stress of the notch (σ_n) vs. applied displacement curves of the AM specimen, and those treated by LSP and HSP obtained during in-situ tensile tests. The static mechanical properties of the three specimens were similar in both the elastic and plastic regions. As expected, the maximum nominal stress of the notched specimens was lower than for the unnotched specimen (see Fig. 3), which had a rupture stress of 500 MPa. The specimen treated by LSP reached a nominal stress of 462 MPa. The maximum nominal stress was slightly lower for the AM specimen (456 MPa) and the specimen treated by HSP (447 MPa). The fracture surface of the tested specimens can be seen in Fig. 4b. This fracture analysis was focused close to the notch, since the maximum local stresses arise within this region during loading. The nominal stress vs. displacement curves of the three specimens showed a similar behaviour, due to the fact that machining and SP only affect a small region near the surface of the cross section of the specimen [35]. However, the fracture analysis revealed differences near the notch of the three surface conditions. Both shot-peened surfaces underwent a primarily ductile fracture, as evidenced by the highly deformed dimples on the surface. However, the AM specimen developed a brittle fracture near the notch prior to the ductile fracture. Although this brittle behaviour did not affect the macroscopic tensile behaviour, it can be detrimental for the fatigue resistance of the material.

4.3. Initial state after shot peening

Fig. 5a shows the $\varepsilon_{220,x}$ strain maps in the AM, LSP and HSP notches at the initial state. The strain distribution was relatively symmetrical, but non-homogenous, around the area of the notch for the three conditions. Table 3 compares the initial longitudinal strains ($\varepsilon_{220,x}$) in the flat surface (point A), in the edge of the notch at 0.3 mm from the flat surface (point B) and at the notch tip (point C), as identified in Fig. 5a. The milling process induced compressive residual longitudinal strains near the flat surface (point A), but tensile strains were generated when contouring the notch. In contrast, both LSP and HSP induced compressive strains in the flat surface and at the notch tip, whereas tensile strains were measured near point B. The magnitude of compressive strains induced by peening at the notch tip, where the maximum in-service stresses occur, was ~30 % higher than in the flat surface. Besides that, the depth of the compressive strains near the notch was similar for LSP and HSP, i.e. ~0.4–0.5 mm from the surface, the compressive strain distribution in the HSP was wider than in LSP. In contrast, LSP induced ~30 % higher compressive strains than HSP close to the notch tip.

The experimental values of the FWHM can serve to track local plastic deformation effects and their evolution during testing [29]. Fig. 6a shows the initial FWHM distribution in the AM, LSP and HSP notched specimens, normalised to the $FWHM_0$ value of the core material in the unstrained state averaged over positions 1.5–2 mm from the notch surface, i.e. $FWHM/FWHM_0$. The distribution of $FWHM/FWHM_0$ around the notch is relatively homogenous in the three tested surface conditions. The intensity and thickness of the layer with higher $FWHM/FWHM_0$ values, and consequently higher local plastic deformation, is located near the notch tip in the three surface states. Some data points close to the edge show abnormally high values ($FWHM/FWHM_0 > 2$) due to the statistics of the measurement where the X-ray beam only partially illuminated the specimen. Despite these limitations at the specimen edge, the in-depth distribution remains reliable. The layer affected by an increase in FWHM, and thus in plastic deformation, had an average thickness of ~0.2–0.3 mm around the notch of the AM specimen, with $FWHM/FWHM_0$ ranging from 1.4 to 1.7 near the surface. The specimen treated by LSP shows a thicker plastically deformed layer (~0.3–0.4 mm) around the notch, with $FWHM/FWHM_0$ ranging from 1.5 to 1.8 near the surface. Increasing the shot peening intensity led to a thicker plastically deformed layer ~0.4–0.6 mm around the notch, and with higher $FWHM/FWHM_0$ values, ranging from 1.6 to 1.8 within the first 0.2 mm near the surface.

4.4. In-situ SXRD upon loading

Fig. 5 shows $\varepsilon_{220,x}$ strain distributions of the AM, LSP and HSP notched specimens at the initial state, and also for an intermediate and high applied nominal stress. The maximum absolute strain values were reached near the notch tip. When applying an intermediate load, the maximum tensile strain was detected at the tip surface of the AM notch, but it was located beneath the surface in both LSP and HSP surfaces. At the highest load, the maximum strain also shifted beneath the surface in the AM specimen. In contrast, strain values barely changed upon loading near the flat region. Since the highest stresses are expected near the

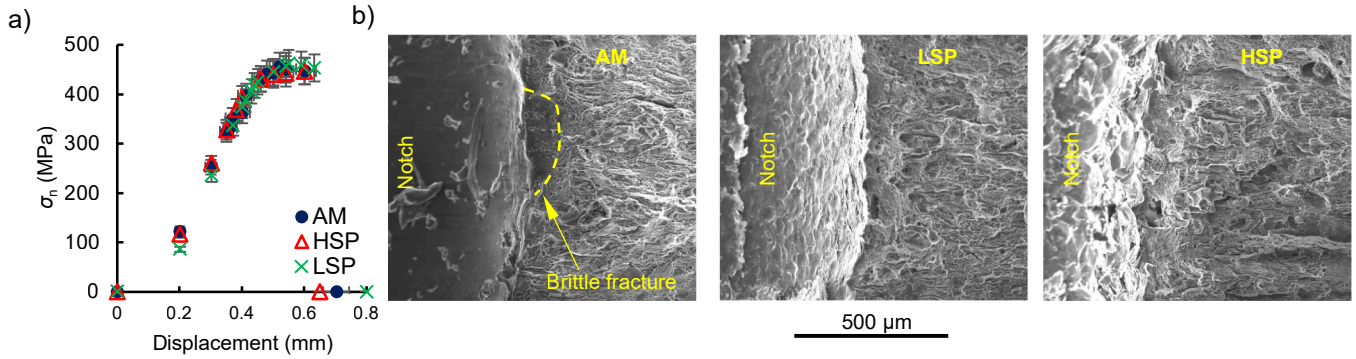

Fig. 4. (a) Nominal stress of the notch as function of applied displacement obtained during in-situ tensile tests and (b) secondary electron images of the fracture surface of the As-Machined (AM), Low (LSP) and High intensity Shot Peening (HSP) specimens.

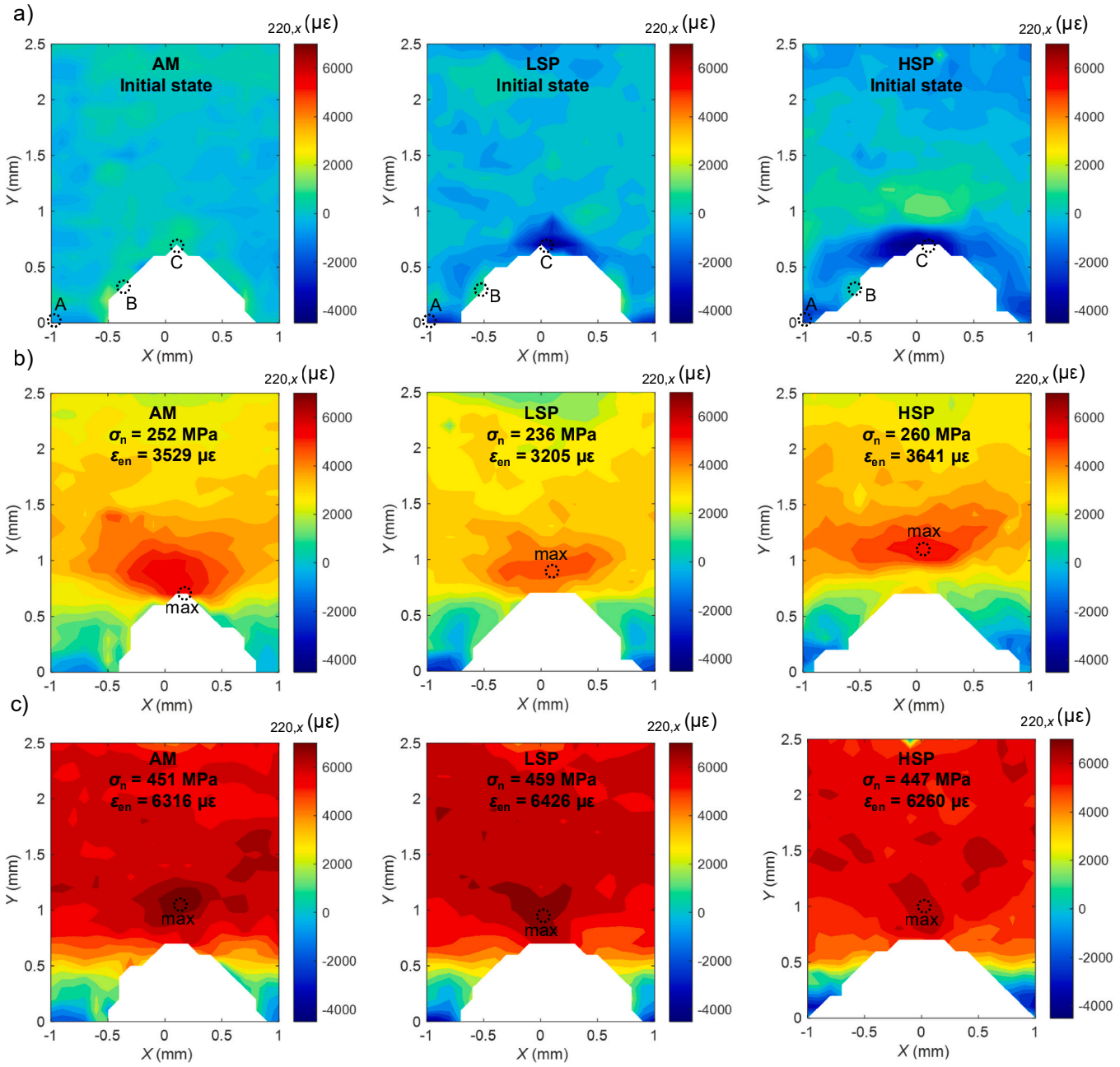

Fig. 5. Distribution of experimental values of the $\varepsilon_{220,x}$ elastic strains in the As-Machined (AM), Low (LSP) and High intensity Shot Peening (HSP) notches (a) in the initial state, and at a (b) intermediate and (c) high applied nominal stress. Nominal stress (σ_n) and elastic strain (ε_{en}) are shown in each map.

Table 3
Longitudinal lattice strains ($\varepsilon_{220,x}$) at selected positions A, B and C (see labelling in Fig. 5a), prior to the start of the in-situ SXRD experiment under loading.

Surface condition	$\varepsilon_{220,x}$ (με)		
	A	B	C
AM	−694 ± 60	758 ± 235	653 ± 51
LSP	−2923 ± 65	1137 ± 21	−3733 ± 210
HSP	−2231 ± 262	420 ± 144	−2861 ± 224

notch tip, a more detailed analysis was done in this region. Fig. 7 compares the evolution of the longitudinal strain along the bisector of the notch upon loading, based on the FEM simulations (7a) and SXRD results (7b-d). The longitudinal elastic strain ε_x in the simulations was calculated by subtracting the plastic longitudinal strain from the total longitudinal strain.

The milling process induced relatively low residual strains. Therefore, the behaviour of the AM notch during loading (Fig. 7b) would be comparable to the FEM simulation where no initial strains were included (Fig. 7a). This assumption is confirmed in Figs. 7a and 7b, since the data in both graphs follow the same qualitative trends upon tensile loading the specimen. In both cases, the longitudinal strains significantly increased near the surface when applying low or medium nominal stress ($\sigma_n > 275$ MPa). Further increase of the applied nominal stress shifted the maximum strain position beneath the surface. The FEM simulation predicted higher surface longitudinal elastic strains than the AM notch experiment, and also a higher shift in the position of the maximum strains.

The maximum compressive strain was located at the notch tip of the LSP specimen at the initial state, Fig. 7c. When applying low nominal

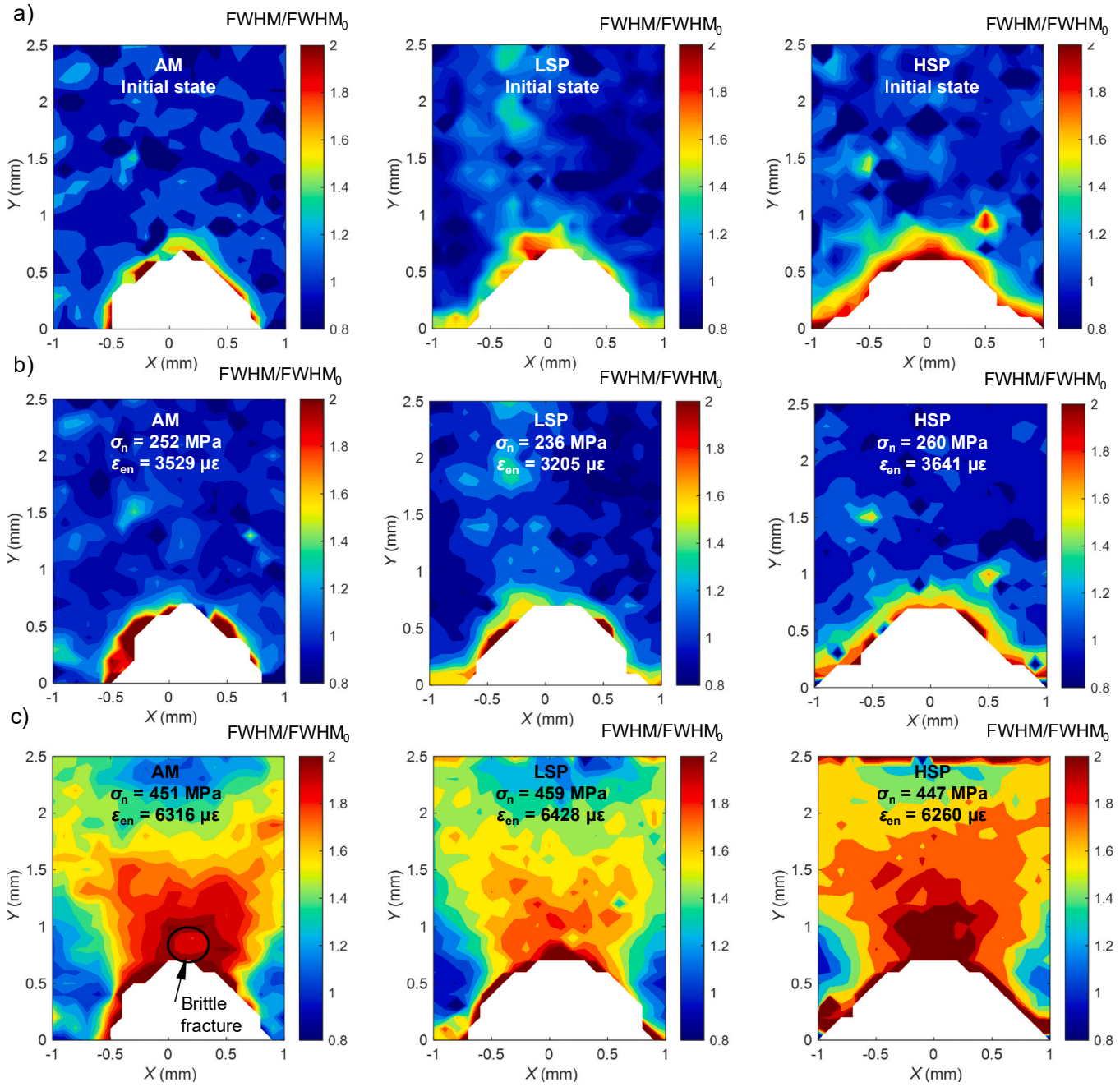

Fig. 6. Distribution of the Full-Width-at-Half-Maximum (FWHM), normalised to its value at zero applied stress in the core material ($FWHM_0$), in the As-Machined (AM), Low (LSP) and High intensity Shot Peening (HSP) notches (a) in the initial state, and at a (b) intermediate and (c) high applied nominal stress. Nominal stress (σ_n) and elastic strain (ε_{en}) are shown in each map.

stresses, the maximum compressive strain was still at the notch tip, but the difference with respect to the bulk strain value was reduced. Despite the stress concentration factor of the notch, medium applied nominal stresses (e.g. 236 MPa) did not induce maximum tensile strains at the notch tip. The longitudinal strains distribution of the specimens treated by HSP followed a similar trend, Fig. 7d. The minimum strain was located beneath the notch tip (depth from the flat surface = 0.8 mm) at low and medium applied stresses, and the maximum elastic strain was found at inner positions. The distribution and magnitude of the longitudinal elastic strains for both LSP and HSP at high applied stress was similar and also comparable to the FEM simulations.

The accumulation of plastic deformation around the notches during loading can be observed in Fig. 6. The distribution of $FWHM/FWHM_0$ in the initial state (Fig. 6a) and intermediate load (Fig. 6b) was almost the same, which suggests that no further plastic deformation was accumulated. As discussed in Section 4.3, the high values observed in the edge of the notch are due to the statistics of the measurements, which is also further affected by the contraction caused by the Poisson effect. The accumulated plastic deformation can be evidenced at high applied nominal stresses (Fig. 6c). The highest values are observed near the notch tip, which also match with the lattice strain distribution measured in this region. By contrast, the $FWHM/FWHM_0$ ratio did not vary from the initial state near the flat region of the specimen, and therefore no plastic deformation was developed in that region. The final qualitative distribution of $FWHM/FWHM_0$ in the LSP and HSP notch was similar, with the highest values near the notch tip. However, the AM specimen showed a decrease $FWHM/FWHM_0$ near the notch (circled with dots in Fig. 6c, left) compared to the peak region beneath the surface. This

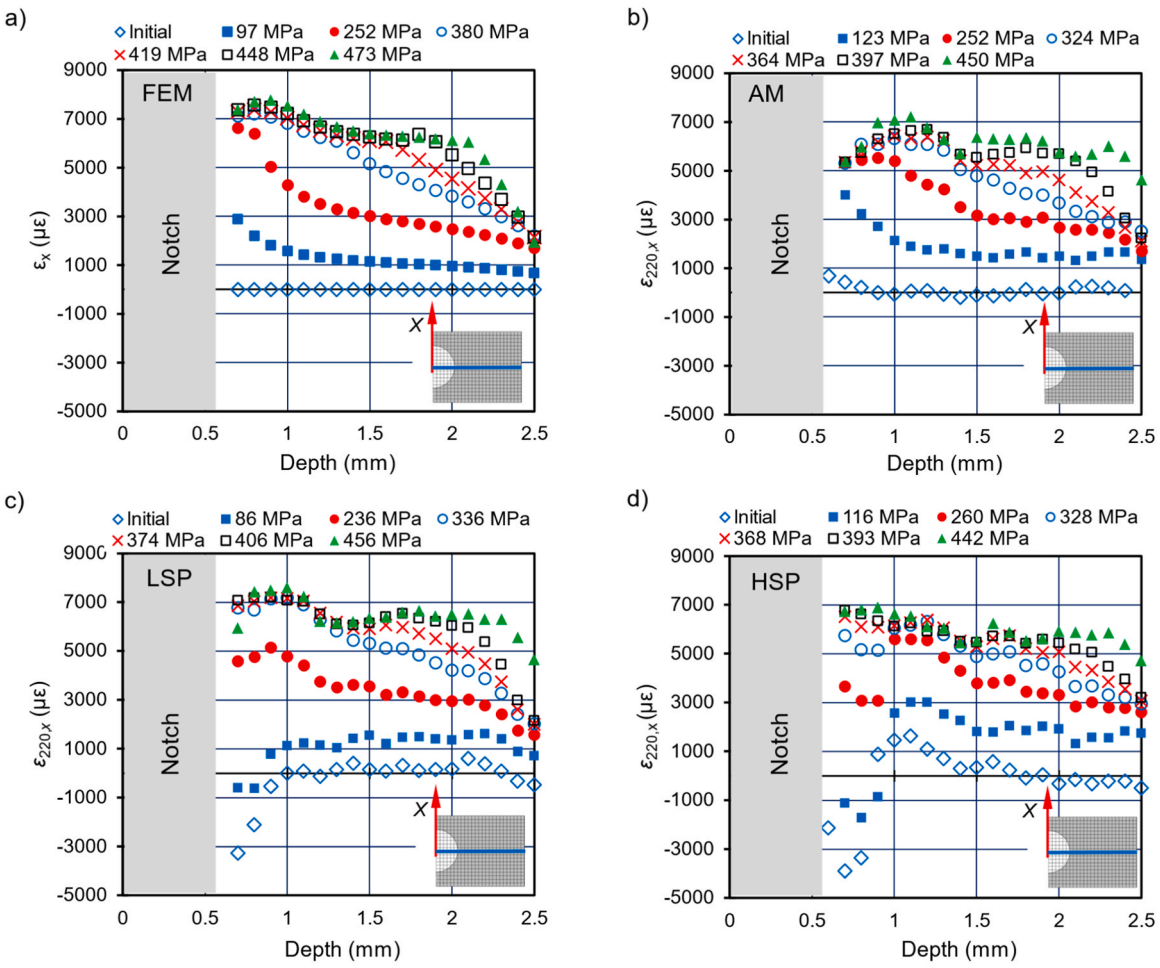

Fig. 7. Evolution of longitudinal strains along the bisector of the notch during tensile loading, obtained from (a) FEM simulations, and from the diffraction experiment for the (b) As-Machined (AM), (c) Low (LSP) and (d) High intensity Shot Peening (HSP) specimens.

suggests that less plastic deformation was accumulated in that region, possibly due to the brittle fracture observed in Fig. 4b.

5. Discussion

5.1. Lattice strain evolution at shot-peened notches

Fig. 8a shows the evolution of longitudinal lattice strains at the surface of the notch tip ($\varepsilon_{surf,x}$) as function of the applied nominal stress, based on the FEM simulation and SXRD experiment. For nominal applied stresses $\sigma_n < 175$ MPa, the three experimental datasets and the FEM simulation show the same linear response. This implies that the surface affected by machining and by SP have similar elastic moduli to the base material, i.e. a value of $E = 71.4$ GPa, which was used in the FEM simulations. Chen et al. [22] did not find significant changes either in the elastic modulus of ferrite and austenite after shot peening SAF2507 duplex stainless steel. However, yielding of the surface occurs at a different applied nominal stress in each case. The surface of the FEM starts yielding at 197 MPa, reaching $\varepsilon_{surf,x} \approx 6300$ με. The surface of the notch treated by LSP begins to yield at higher loads than the unpeened case, i.e at 335 MPa nominal applied stress, and also reaches slightly higher strains, $\varepsilon_{surf,x} \approx 6750$ με. Similarly, the notch treated by HSP yields at 360 MPa and $\varepsilon_{surf,x} \approx 6500$ με. This increase in the range of elastic behaviour is due to the compressive residual strains induced by SP. Consequently, the maximum tensile load that we can apply in SP surfaces, before yielding occurs, is 70–80 % higher than without the surface treatment. By contrast, the as-machined surface only shows an elastic behaviour up to 175 MPa applied nominal stress, and the maximum strain reached by this surface is the lowest of the experimental tests.

Although the surface of the notch tip of the tested and simulated conditions start to yield at a different stress and reach different strains, they converge at the same surface elastic strain (6900–7200 με) when applying higher loads, see Fig. 8a. The maximum surface elastic strain does not increase significantly with respect to the surface strain at yielding, and therefore strain hardening is low. However, the surface strains in the AM notched specimen did not increase at high loads, potentially due to crack nucleation and propagation close to the notch, as evidenced by the brittle fracture in Fig. 4b. Besides that, the surface strain in the LSP notched specimen decreased at the highest load, which may indicate that the crack formation before final specimen fracture. Based on in-situ mechanical tests combined with laboratory-based X-ray diffraction, other researchers have reported an increase of 210–250 % in the local yield stress of the SP-affected layer compared to the bulk properties in in X42Cr13 and 55Si7 steels [36], ~300 % in S30432 austenitic steel [20], 27 % in Ti6Al4V [21], and an increase of 59 % and 104 % in the local yield stress of ferrite and austenite after shot peening SAF2507 duplex stainless steel [22]. Those significant increases were mainly attributed to the grain refinement (Hall-Petch effect) and increased dislocation density. Nevertheless, Biancheti et al. [23] only determined around 10 % increase in the yield stress of shot-peened aluminium alloy 7050-T7451 through the relationship of FWHM and strain, which confirms that this material is not prone to work harden. In fact, the aluminium-base 7050-T7451 alloy possesses only a slight strain

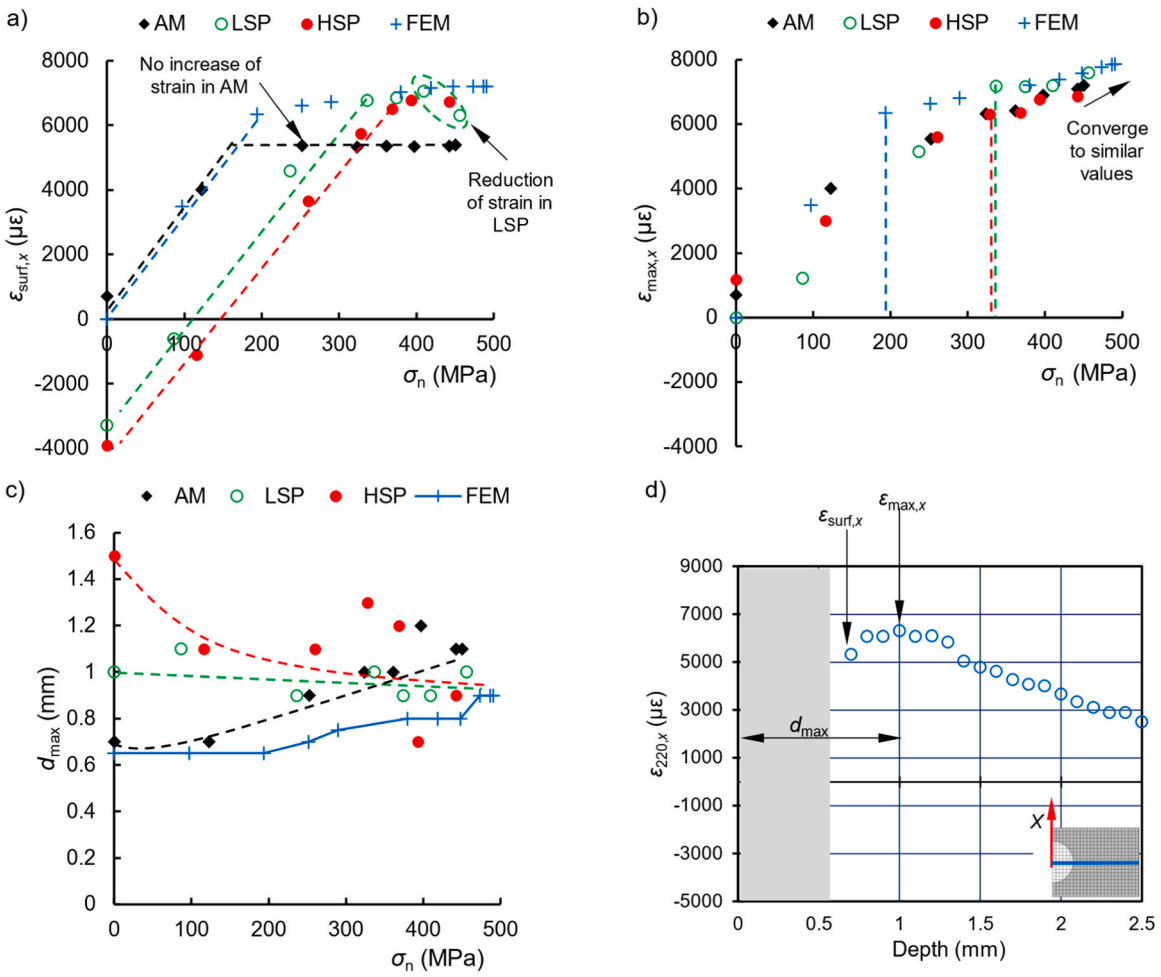

Fig. 8. Variation with the applied nominal stress of the (a) longitudinal elastic strain at the surface of the notch tip ($\varepsilon_{surf,x}$), (b) maximum longitudinal elastic strain along the bisector of the notch ($\varepsilon_{max,x}$), and (c) position of the maximum longitudinal elastic strain with respect to the specimen surface (d_{max}). The parameters used in (a-c) are schematically defined in (d) for the longitudinal elastic strain measured in AM specimen when applying a 324 MPa nominal stress.

rate sensitivity at room temperature [37,38], due to the hindrance of local precipitates to dislocation motion [37].

The maximum longitudinal elastic strain $\varepsilon_{max,x}$ along the bisector and the depth of its location d_{max} as function of the applied nominal stress are shown in Fig. 8b & 8c, respectively. The schematic in Fig. 8d identifies those parameters. The maximum strain increases until it reaches $\varepsilon_{surf,x} \approx$ 6300–6700 με. At this point, yielding occurs and the elastic strains increase smoothly with further increase in applied stress. The experimental and simulated datasets converge to the same value. This suggests that the rupture stress of aluminium 7050-T7451 is not affected by the intensity of the peening process. In the absence of residual strains (FEM simulations) or presence of tensile residual strains (AM specimen), the maximum longitudinal surface elastic strain is located at the notch tip until yielding starts. In contrast, the highest tensile residual elastic strain is located at 1.6 mm depth in the HSP notch, but the position of the maximum tensile strain rapidly shifts closer to the surface as consequence of the stress concentration factor as shown in the variation of d_{max} with the nominal stress σ_n in Fig. 8c. The position of the maximum longitudinal elastic strains is more stable in the LSP notch, since it is at ~1 mm depth from the flat surface for the whole range of applied stresses. The position of the maximum strain converges to the same point, ≈ 1 mm depth from the flat surface when increasing the applied nominal stress.

5.2. Local plastic effects

Fig. 9a compares the evolution of $FWHM_{surf}/FWHM_0$ measured in the SXRD experiment and the plastic strain determined in FEM simulations with the applied nominal stresses. $FWHM_{surf}/FWHM_0$ reduces during the elastic regime, due to the accommodation of the dislocations initially generated by milling and SP. This effect has also been observed by Zhong et al. [39] in aluminium alloy 7020-T6, the applied stresses are not enough to activate dislocation slips in the elastic regime, but can make move pre-existing dislocations. Consequently, when dislocation line segments of opposite polarity interact, they can arrange in lower-energy configurations or annihilate each other, reducing the dislocation density. Once the notch surface starts yielding, $FWHM_{surf}/FWHM_0$ increases exponentially as function of the applied stress. The FEM simulations also predict a similar behaviour for the unstrained notch, with the plastic strain increasing exponentially at $\sigma_n > 200$ MPa. Therefore, this confirms that the FWHM is a good indicator of the accumulated plastic strains [29]. As for the maximum longitudinal elastic strain, the LSP notch shows a slight reduction of the $FWHM_{surf}/FWHM_0$ at the highest applied load, which could indicate the nucleation of a crack or initiation of the final material's fracture.

The changes in $FWHM_{max}/FWHM_0$ at the most strained point measured in the SXRD experiment and the plastic strain determined in FEM simulation as function of the applied stress can be seen in Fig. 9b. The position of the most strained point for each surface condition and loading step is shown in Fig. 8c. There is no significant increase of

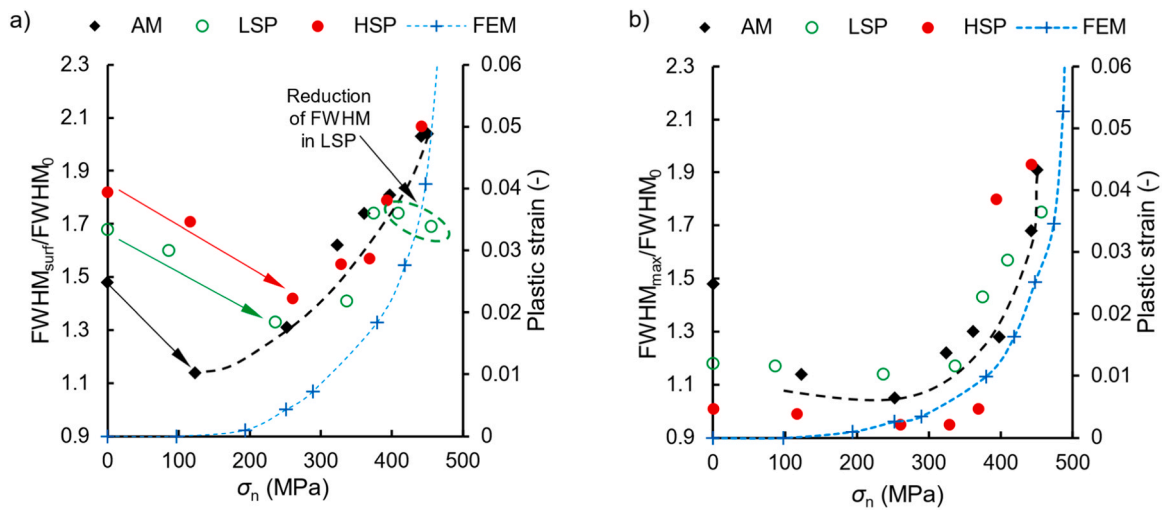

Fig. 9. Evolution with the applied nominal stress of the (a) full width at half maximum at the surface of the notch tip ($FWHM_{surf}$) and (b) full width at half maximum at the most strained point in the experiment ($FWHM_{max}$), both normalised to its value at zero applied stress ($FWHM_0$), together with the plastic strain determined in the FEM simulations. The experimental values were obtained for the As-Machined (AM), Low (LSP) and High intensity Shot Peening (HSP) specimens.

$FWHM_{max}/FWHM_0$ or plastic strain up to $\sigma_n \approx 300$ MPa in all the tested conditions. Further increase of the applied nominal stress exponentially rises the $FWHM_{max}/FWHM_0$ obtained in the experiments (black dotted line) and the plastic strain predicted in simulations. Furthermore, at $\sigma_n \approx$ 300 MPa $FWHM_{max}/FWHM_0$ is lower than $FWHM_{surf}/FWHM_0$, but at the highest applied nominal stress the $FWHM_{max}/FWHM_0$ ratios show a similar value, as well as the FEM plastic strain.

The fatigue strength of shot-peened notched specimens can be estimated using the theory of critical distance [5,10,13,15,34]. In a recent work, Benedetti et al. [34] demonstrated that including only surface roughness and residual stress field is enough to satisfactorily model the fatigue behaviour of aluminium 7075-T6 shot-peened specimens, since grain refinement and work hardening have a marginal effect, which agrees with the results of the present work. The methodology presented in this paper has been satisfactorily employed to map the elastic strain distribution and plastic deformation accumulation around unpeened and peened notches at the initial state and upon loading up to fracture. The experimental values of the local strain field can support FEM simulations in reconstructing the residual stress field around the notch using eigenstrains [18], and thereupon predict the fatigue strength of shot-peened notched specimens by TCD [10,13,15,34]. Therefore, future work will focus on the characterised residual strain fields in shot-peened notched specimens, and simulating and experimenting the fatigue performance for high cycle fatigue (HCF) and low cycle fatigue (LCF) conditions. We expect that the compressive residual stresses induced by shot peening will not relax during cyclic loading in HCF regime because of the lower local stress (compressive residual stress + applied stress) than the yield stress, and consequently will increase the fatigue strength. However, the positive effect of shot peening could be significantly reduced in the LCF regime where plastic strains are induced, because i) our results show that the local yield stress of the shot peening affected layer was not increased, and ii) shot peening affected layer still accumulated plastic strain upon loading. Furthermore, to the best of authors knowledge, this is the first time that residual strains induced by shot peening are experimentally mapped around notches with sufficient spatial resolution, and the experimental values from this work are key to validate numerical models of shot peening process conducted on geometrical features. The development of such models would reduce the required experimental work to characterise residual stresses through additional sophisticated experiments.

6. Conclusions

This work has probed the evolution of local strain fields of machined and shot-peened notches in the aerospace 7050-T7451 alloy, by combining in-situ tensile testing and hard X-ray μ-diffraction in transmission mode and supported by FEM simulations of the non-peened notched specimen. The main conclusions are:

- Shot peening induces near-surface plastic deformation and alterations in the notch geometry as compared to the as-machined state. Additionally, high intensity shot peening produces rougher surfaces and a ~15 μm thick layer with severe plastic deformation in the microstructure near the notch tip.
- The residual strains generated by machining and shot peening are not homogenous around the notch. Importantly, shot peening induces the highest compressive longitudinal strains near the notch tip, where maximum stresses arise in service conditions. The thickness of the compressed layer increases with the peening intensity.
- The notches treated by low intensity and high intensity shot peening withstand 70–80 % higher nominal tensile stresses than the as-machined material before local yielding occurs at the surface of the notch tip.
- The surface elastic strains measured in the SXRD experiment and FEM simulation are similar for the peening and untreated conditions at high applied nominal stresses. This confirms that the local mechanical strength of the aluminium alloy 7050-T7451 was not modified by the peening process in the surface layer.
- The location of the point with maximum longitudinal elastic strains shifts from the surface to inner layers as the applied nominal stress increases for the as-machined notched specimen. At high loads, the position of the most strained point and the magnitude of the maximum elastic strain converges for the three studied cases.
- The evolution of FWHM measured in the experiments and the FEM-predicted plastic strains as function of the applied nominal stress follow the same trend. This analysis demonstrates that plastic strain accumulates exponentially when increasing the applied nominal stress once yielding occurs. Additionally, the shot-peened notches experience local plastic damage accommodation at the early stages of the tensile test.

CRediT authorship contribution statement

A. Madariaga: Conceptualization, Methodology, Investigation,

Formal analysis, Writing - original draft. **E. Vazquez:** Investigation, Resources, Writing - review & editing. **D. Foster:** Investigation, Writing - review & editing. **E. Jimenez-Melero:** Conceptualization, Methodology, Investigation, Supervision, Resources, Writing - review & editing.

Declaration of Competing Interest

The authors declare that they have no known competing financial interests or personal relationships that could have appeared to influence the work reported in this paper.

Acknowledgments

This work was funded through the LOFAMO grant from EPSRC [EP/X023281/1]. We also acknowledge the Diamond Light Source for the allocation of beamtime on the I12 instrument under proposal Experiment MG24327–1, and the Electron Microscopy Centre of the University of Manchester. EJM thanks the UKAEA funding of his Joint Chair position in Materials for Fusion in Birmingham through the EPSRC Energy Programme [EP/W006839/1].

Appendix A. Supporting information

Supplementary data associated with this article can be found in the online version at doi:10.1016/j.jallcom.2025.182861.

Data availability

Data will be made available on request.

References

[1] S. Bagherifard, Enhancing the structural performance of lightweight metals by shot peening, Adv. Engin. Mater. 21 (7) (2019) 1801140.
[2] ASM handbook, Properties and selection: nonferrous alloys and special purpose materials, 10th ed., 2, American Society for Metals, Materials Park (OH), 1991.
[3] J.C. Bian, K. Tokaji, T. Ogawa, Notch sensitivity of aluminium-lithium alloys in fatigue, Fatigue Fract. Engin. Mater. Struct. 18 (1) (1995) 119–127.
[4] K. Oguri, Fatigue life enhancement of aluminum alloy for aircraft by fine particle shot peening (FPSP), J. Mater. Proc. Technol. 211 (8) (2011) 1395–1399.
[5] M. Benedetti, V. Fontanari, M. Bandini, A simplified and fast method to predict plain and notch fatigue of shot peened high-strength aluminium alloys under reverse bending, Surf. Coat. Technol. 243 (2014) 2–9.
[6] Y. Austernaud, M. Novelli, P. Bocher, T. Grosdidier, Effect of shot peening temperature on the microstructure induced by surface severe plastic deformation on an austenitic stainless steel, J. Mater. Proc. Technol. 339 (2025) 118823.
[7] L. Bao, K. Li, J. Zheng, Y. Zhang, K. Zhan, Z. Yang, B. Zhao, V. Ji, Surface characteristics and stress corrosion behavior of AA 7075-T6 aluminum alloys after different shot peening processes, Surf. Coat. Techn 440 (2022) 128481.
[8] Y. Mutoh, G.H. Fair, B. Noble, R.B. Waterhouse, The effect of residual stresses induced by shot-peening on fatigue crack propagation in two high strength aluminium alloys, Fatigue Fract. Engin. Mater. Struct. 10 (4) (1987) 261–272.
[9] Y.K. Gao, X.R. Wu, Experimental investigation and fatigue life prediction for 7475-T7351 aluminum alloy with and without shot peening-induced residual stresses, Acta Mater. 59 (9) (2011) 3737–3747.
[10] S. Bagherifard, C. Colombo, M. Guagliano, Application of different fatigue strength criteria to shot peened notched components. Part 1: fracture mechanics based approaches, Appl. Surf. Sci. 289 (2014) 180–187.
[11] M. Benedetti, V. Fontanari, C. Santus, M. Bandini, Notch fatigue behaviour of shot peened high-strength aluminium alloys: experiments and predictions using a critical distance method, Int. J. Fatigue 32 (10) (2010) 1600–1611.
[12] M. Benedetti, V. Fontanari, M. Allahkarami, J.C. Hanan, Notch fatigue behaviour of shot peened high-strength aluminium alloys: role of the residual stress field ahead of the notch root. In Experimental and Applied Mechanics, Volume 6: Proc. of the 2014 Annual Conf. on Experimental and Applied Mechanics, Springer International Publishing, 2015, pp. 113–121.
[13] M. Benedetti, V. Fontanari, B. Winiarski, P.J. Withers, M. Allahkarami, J.C. Hanan, Fatigue behavior of shot peened notched specimens: effect of the residual stress field ahead of the notch root, Proc. Engin 109 (2015) 80–88.
[14] M. Jambor, L. Trško, J. Klusák, S. Fintová, D. Kajánek, F. Nový, O. Bokůvka, Effect of severe shot peening on the very-high cycle notch fatigue of an AW 7075 alloy, Metals 10 (9) (2020) 1262.
[15] S. Bagherifard, M. Guagliano, Application of different fatigue strength criteria on shot peened notched parts. Part 2: nominal and local stress approaches, Appl. Surf. Sci. 289 (2014) 173–179.
[16] M. Marini, V. Fontanari, M. Benedetti, DEM/FEM simulation of the shot peening process on sharp notches, Int. J. Mech. Sci. 204 (2021) 106547.
[17] B. Winiarski, M. Benedetti, V. Fontanari, M. Allahkarami, J.C. Hanan, P.J. Withers, High spatial resolution evaluation of residual stresses in shot peened specimens containing sharp and blunt notches by micro-hole drilling, micro-slot cutting and micro-X-ray diffraction methods, Exp. Mech. 56 (2016) 1449–1463.
[18] M. Benedetti, V. Fontanari, B. Winiarski, M. Allahkarami, J.C. Hanan, Residual stresses reconstruction in shot peened specimens containing sharp and blunt notches by experimental measurements and finite element analysis, Int. J. Fatigue 87 (2016) 102–111.
[19] S. Coratella, M. Sticchi, M.B. Toparli, M.E. Fitzpatrick, N. Kashaev, Application of the eigenstrain approach to predict the residual stress distribution in laser shock peened AA7050-T7451 samples, Surf. Coat. Technol. 273 (2015) 39–49.
[20] K. Zhan, C.H. Jiang, V. Ji, Surface mechanical properties of S30432 austenitic steel after shot peening, Appl. Surf. Sci. 258 (24) (2012) 9559–9563.
[21] L. Xie, Y. Wen, K. Zhan, L. Wang, C. Jiang, V. Ji, Characterization on surface mechanical properties of Ti–6Al–4V after shot peening, J. Alloy. Comp. 666 (2016) 65–70.
[22] M. Chen, S. Xing, H. Liu, C. Jiang, K. Zhan, V. Ji, Determination of surface mechanical property and residual stress stability for shot-peened SAF2507 duplex stainless steel by in situ X-ray diffraction stress analysis, J. Mater. Res. Technol. 9 (4) (2020) 7644–7654.
[23] C. Bianchetti, D. Delbergue, P. Bocher, M. Lévesque, M. Brochu, Analytical fatigue life prediction of shot peened AA 7050-T7451, Int. J. Fatigue 118 (2019) 271–281.
[24] A. Steuwer, J.E. Daniels, M.J. Peel, In situ crack growth studies of hydrided Zircaloy-4 on a single-edge notched tensile specimen, Scr. Mater. 61 (4) (2009) 431–433.
[25] A. Steuwer, M. Rahman, A. Shterenlikht, M.E. Fitzpatrick, L. Edwards, P.J. Withers, The evolution of crack-tip stresses during a fatigue overload event, Acta Mater. 58 (11) (2010) 4039–4052.
[26] P. Lopez-Crespo, A. Steuwer, T. Buslaps, Y.H. Tai, A. Lopez-Moreno, J.R. Yates, P. J. Withers, Measuring overload effects during fatigue crack growth in bainitic steel by synchrotron X-ray diffraction, Int. J. Fatigue 71 (2015) 11–16.
[27] P. Zheng, R. Chen, H. Liu, J. Chen, Z. Zhang, X. Liu, Y. Shen, On the standards and practices for miniaturized tensile test–A review, Fusion Eng. Des. 161 (2020) 112006.
[28] SAE International, Shot peening coverage determination, SAE Stand, 2023, p. J2277.
[29] A. Madariaga, E. Vázquez, D. Foster, E. Jimenez-Melero, Depth-resolved mechanical behaviour of shot peened 7050-T7451 aluminium surfaces using in-situ synchrotron X-ray diffraction, Mater. Sci. Engin. A 909 (2024) 146817.
[30] M.L. Hart, M. Drakopoulos, C. Reinhard, T. Connolley, Complete elliptical ring geometry provides energy and instrument calibration for synchrotron-based two-dimensional X-ray diffraction, J. Appl. Cryst. 46 (5) (2013) 1249–1260.
[31] J. Filik, A.W. Ashton, P.C.Y. Chang, P.A. Chater, S.J. Day, M. Drakopoulos, M. W. Gerring, M.L. Hart, O.V. Magdysyuk, S. Michalik, A. Smith, Processing two-dimensional X-ray diffraction and small-angle scattering data in Dawn 2, J. Appl. Cryst. 50 (3) (2017) 959–966.
[32] J. Rodriguez-Carvajal, FULLPROF: a program for rietveld refinement and pattern matching analysis. Abstracts of the Satellite Meeting on Powder Diffraction of the XV Congress of the IUCr, Toulouse, France, 1990, p. 127 (1990).
[33] I. Perez, A. Madariaga, M. Cuesta, A. Garay, P.J. Arrazola, J.J. Ruiz, F.J. Rubio, R. Sanchez, Effect of cutting speed on the surface integrity of face milled 7050-T7451 aluminium workpieces, Procedia Cirp 71 (2018) (2018) 460–465.
[34] M. Benedetti, M. Pedranz, V. Fontanari, C. Menapace, M. Bandini, Enhancing plain fatigue strength in aluminum alloys through shot peening: experimental investigations and a strain energy density interpretation, Int. J. Fatigue 184 (2024) 108299.
[35] S. Aguado-Montero, J. Vázquez, C. Navarro, J. Domínguez, Fatigue behavior of notched and unnotched AM scalmalloy specimens subjected to different surface treatments, Int. J. Fatigue 181 (2024) 108146.
[36] J.P. Nobre, A.C. Batista, L. Coelho, A.M. Dias, Two experimental methods to determining stress–strain behavior of work-hardened surface layers of metallic components, J. Mater. Process. Technol. 210 (2010) 2285–2291.
[37] F. Jiang, J. Li, J. Sun, S. Zhang, Z. Wang, L. Yan, Al7050-T7451 turning simulation based on the modified power-law material model, Int. J. Adv. Manuf. Technol. 48 (2010) 871–880.
[38] G. Chen, C. Ren, Z. Ke, J. Li, X. Yang, Modeling of flow behavior for 7050-T7451 aluminum alloy considering microstructural evolution over a wide range of strain rates, Mech. Mater. 95 (2016) 146–157.
[39] Z.Y. Zhong, H.G. Brokmeier, W.M. Gan, E. Maawad, B. Schwebke, N. Schell, Dislocation density evolution of AA 7020-T6 investigated by in-situ synchrotron diffraction under tensile load, Mater. Charact. 108 (2015) 124–131.